論文 / 著書情報
Article / Book Information

Title	Direct visualization of polarization reversal of organic ferroelectric memory transistor by using charge modulated reflectance imaging
Authors	Takako Otsuka, Dai Taguchi, Takaaki Manaka, Mitsumasa Iwamoto
Citation	Journal of Applied Physics, Volume 122, 18, 185501
Pub. date	2017, 11
Note	This article may be downloaded for personal use only. Any other use requires prior permission of the author and AIP Publishing. The following article appeared in Journal of Applied Physics, Volume 122, 18, 185501 and may be found at https://doi.org/10.1063/1.5004002.
Note	This file is author (final) version.

Direct visualization of polarization reversal of organic ferroelectric memory transistor by using charge modulated reflectance imaging

Takako Otsuka, Dai Taguchi, Takaaki Manaka, and Mitsumasa Iwamoto*

Department of Physical Electronics, Tokyo Institute of Technology,

2-12-1, O-okayama, Meguro-ku, Tokyo 152-8552 Japan

Abstract

By using charge modulated reflectance (CMR) imaging technique, charge distribution in the pentacene organic field-effect transistor (OFET) with a ferroelectric gate insulator [P(VDF-TrFE)] was investigated in terms of polarization reversal of the P(VDF-TrFE) layer. We studied the polarization reversal process and carrier spreading process in the OFET channel. I-V measurement showed a hysteresis behavior caused from the spontaneous polarization of P(VDF-TrFE), but the hysteresis I-V curve changes depending on the applied drain bias, possibly due to the gradual shift of polarization reversal position in the OFET channel. CMR imaging visualized the gradual shift of polarization reversal position, and showed that the electrostatic field formed by the polarization of P(VDF-TrFE) contributes to hole and electron injection into pentacene layer and the carrier distribution is significantly dependent on the direction of the polarization. Polarization reversal position in the channel region is governed by the electrostatic potential and it happens where the potential reaches the coercive voltage of P(VDF-TrFE). Transmission line model developed on the basis of the Maxwell-Wagner effect element analysis well accounts for this polarization reversal process in the OFET channel.

Keywords: charge modulation spectroscopy, polarization reversal, organic semiconductor, charge-dipole interaction, memory transistor

1. Introduction

Since the discovery of electrical conducting organic materials, much attention has been paid to the development of organic devices, e.g. organic field-effect transistors (OFETs) [1], organic light-emitting diodes (OLEDs) [2], organic solar cells (OSCs) [3], organic memory devices [4], etc., by utilizing advantageous features of organic materials such as weight lightness, mechanical flexibility, easy-process ability, etc [5,6]. At the initial research stage of OFETs, the effective carrier mobility was quite low [7], but nowadays we can see OFETs whose carrier mobility exceeds $10\,\mathrm{cm}^2/\mathrm{Vs}$ [8,9], due to the emergence of innovative and advanced fabrication techniques based on solution process, molecular evaporation process and so forth [10], and also of new organic semiconductor molecules and synthetic conducting polymers. Nevertheless, there are still many problems to be solved for practical use of organic materials in devices. This situation motivated us to study carrier behaviors in organic devices, on the basis of dielectric physics approach [11-13] that differs from the conventional semiconductor device physics approach [14]. We therefore have been developing a method for analyzing organic devices as Maxwell-Wagner (MW) effect elements [15-19], and also a novel experimental technique for visualizing carrier dynamics in organic devices such as carrier transit in the channel of OFETs [20-22], carrier transit across the double layer of OLEDs [23-25] etc. by using electric field induced optical second harmonic generation (EFISHG) measurement.

In our previous paper, we studied the displacement current–voltage characteristics of metal/ ferroelectric/ organic semiconductor/ metal (MFS) diodes by using the EFISHG measurement [26]. Results showed that the EFISHG measurement coupled with displacement current measurement (DCM) is useful for analyzing the relationship between the polarization reversal process in the ferroelectric layer and associated carrier behaviors in the semiconductor layer, in terms of the three-peak generation in the DCM [27-29]. We also used the charge modulation

spectroscopy (CMS) to study the relationship between the related energetics of carriers in semiconductor layer and polarization reversal in MFS diodes [26]. These results showed that combining EFISHG measurement and CMS provides us a way to study spatial and energetic carrier behaviors in semiconductor layer, which is governed by polarization reversal in MFS diodes. As an extension study of the above MIS and MFS studies, the carrier behaviors of pentacene FET with ferroelectric gate insulator was studied using the DCM [30]. However, we could not make clear the polarization reversal process in ferroelectric layer that occurs in the channel region, though we could discuss the relationship between the polarization reversal and the related DCM peaks, on the basis of Maxwell-Wagner model analysis [31-33]. For the device application, it is very important to make clear the polarization reversal propagation and carrier distribution process in the channel of OFET with ferroelectric gate insulator. There are many ways to study the carrier behaviors in the OFET channel microscopically. Among them are microscopic scanning surface potential measurement [34-36], electric field induced optical second harmonic generation measurement [11,20], PL imaging [37] and others [38-42]. CMS imaging also provides a way to visualize carrier behavior in FET channel [43-45]. This technique is capable of probing carriers located in one of molecular energy states, selectively, by choosing an appropriate probe light wavelength. We therefore can utilize CMS imaging for selectively probing mobile charges in semiconducting layer and dipole charges in ferroelectric layer. These results of CMS imaging will be very useful to discuss the relationship between mobile carriers and ferroelectric property in organic devices. In this study, we used the charge modulated reflectance (CMR) imaging technique, i.e., CMS imaging with reflection optical system, and visualized the carrier distribution in the channel region of pentacene FET with ferroelectric gate insulator. After that, the result of the visualized images is analyzed in terms of the polarization reversal, using a theoretical model based on the MW effect.

2. Experimental

Figure 1(a) shows the structure of pentacene FETs with a ferroelectric gate insulator layer. The Al gate electrode was deposited by vacuum evaporation with a thickness of $50\ \mathrm{nm}$ on cleaned glass substrate. As the ferroelectric gate insulator, we used P(VDF-TrFE) [poly(vinylidene fluoride trifluoroethylene)], one of the most promising organic ferroelectric materials with relatively large remanent polarization and good thermal stability [4,46,47]. Copolymer P(VDF-TrFE) with a molar ratio of 70-30 mol% was dissolved into methyl-ethyl-ketone solvent (concentration: 5 wt%), and it was spin-coated on the glass substrate with gate electrode (thickness: 200 nm). Subsequently, the spin-coated films were annealed in a dry nitrogen atmosphere at $120\ ℃$ for 1 h. After that, a pentacene layer (thickness: 50 nm) and Au electrodes (thickness: 100 nm) were successively deposited by vacuum evaporation, where the process pressure and deposition rate were set at $< 10^{-5}$ Torr and $1\ \mathrm{Å/s}$, respectively. Au was evaporated through a shadow mask to make top contacts as source and drain electrodes. The channel length L and width W were $50\ \mu\mathrm{m}$ and $2\ \mathrm{mm}$, respectively. The standard electrical I-V measurement was carried out in dark with two source meters (Keithley 2400) by using the electrode arrangement displayed in Fig. 1(a).

Charge modulation spectroscopy (CMS) can probe the optical spectrum modulation in response to the change of the energetic structure, which is induced by carrier injection [48,49], photoexcitation etc [50]. In our previous study, we showed that charge modulated reflectance (CMR) imaging technique is available for observing the injected carrier distribution in pentacene FETs [43]. Figure 1(a) shows the experimental setup used for the CMR imaging; White light supplied from a white LED with an intensity $\approx 10\ \mathrm{mW/cm^2}$ was passing through

an objective lens, and it was then focused onto the FET channel perpendicularly at an incident angle of 90°. The spot area was 200 μm in diameter. For the CMR imaging experiment, the reflected light intensity was recorded by using microscope optics with a cooled charge-coupled device sensor (Andor technology: DU 920P-BV). The relative change in the reflection intensity ($\Delta R/R$) was measured, under OFET device operation. For the CMS measurement, the intensity of reflected signal was detected by a spectrograph over the range of wavelength between 400 nm to 900 nm. Note that in this region pentacene absorption peaks appear as shown in Fig. 1(b), whereas the P(VDF-TrFE) film exhibits no absorption. In our previous study, we employed CMS measurement to probe the carrier energetics in ITO/P(VDF-TrFE)/pentacene/Au diodes [26], and showed that the carrier injection into pentacene layer makes a dominant contribution to change the energy structure of the pentacene in the wavelength region between 500 nm and 600 nm. Consequently, microscope observation at a fixed wavelength in this region allows us to visualize the carrier behavior in pentacene layer.

3. Results and Discussion

3-A. I-V characteristics

Figures 2(a) and 2(b) show the current-voltage characteristics ((a) drain current I_{ds} - gate voltage V_{gs} and (b) gate current I_{gs} − gate voltage V_{gs}) as a function of V_{ds}. Figure 2(c) illustrates charge and polarization distribution that accounts for the current-voltage characteristics. In Fig. 1(a), the electric circuit used in the measurement is illustrated. The I_{ds}-V_{gs} characteristics of Fig. 2(a) exhibits a typical p-type semiconductor behavior, but with a hysteresis loop. Fig. 2(b) shows the I_{gs}-V_{gs} characteristics, and for V_d= 0 it is similar to our previous result of metal/ ferroelectric/ semiconductor/ metal (MFS) diode [26]; Two peaks (peaks A and B) appear at nearly symmetric positions of applied gate voltages V_{gs} (V_A =

$-16\,\mathrm{V}, V_B = +14\,\mathrm{V}$) with respect to $V_{gs} = 0\,\mathrm{V}$, and these peaks originate from the displacement current due to the spontaneous polarization reversal of the P(VDF-TrFE) layer. The values of V_A and V_B were in good agreement with the coercive voltage of the P(VDF-TrFE) calculated using the coercive electric field ($E_c = 0.85\,\mathrm{MV/cm}$) [26, 51]. We therefore conclude that the hysteresis observed in the drain current-voltage (I_{ds} - V_{gs}) characteristics of Fig. 2(a) is mainly due to the ferroelectric polarization of the P(VDF-TrFE) gate insulator. In the backward gate bias from $V_{gs} = +40\,\mathrm{V}$ to $-40\,\mathrm{V}$, holes can enter into pentacene layer from source electrode due to the turn-over of internal electric field originated from ferroelectric polarization, i.e., after polarization reversal at $V_A = -16\,\mathrm{V}$, resulting in a steep increase of the drain current for $V_{ds} \neq 0\,V$ (Fig. 2(a)). On the other hand, in the forward gate bias from $V_{gs} = -40\,\mathrm{V}$ to $+40\,\mathrm{V}$, the drain current gradually decreases owing to the decrease of holes supplied from the source, and results in suppression of hole propagation along the channel. Subsequently, after polarization reversal at $V_B = +14\,\mathrm{V}$, holes are totally exhausted from the channel, leading to a transition from on-state to off-state of OFETs (see Fig. 2(a)). Interestingly, additional peaks (peaks A' and B') appear when $V_{ds} \neq 0\,V$, and the peak position A' and B' shifts in accordance with the drain voltage V_{ds}. These are our new findings obtained by using the OFET structure, and possibly they occur due to the gradual shift of polarization reversal position of ferroelectric layer along the FET channel, in association with carrier distributions in the channel. However, this is merely a speculation. To further make clear the details of the peak shift, we need to visualize carrier distribution along the FET channel.

3-B CMR imaging

3-B-1 $V_{ds} = 0\,\mathrm{V}$

As the first step, we focused on the carrier distribution along the OFET channel at zero drain

bias ($V_{ds} = 0$ V). Figure 3 shows the result of CMR imaging, where an optical filter with a center wavelength of 580 nm and a band width of 10 nm was used. Noteworthy that the charge modulation spectrum of pentacene film has a strong peak at a wavelength of 580 nm due to the HOMO-LUMO excitation, and this peak is ascribed to the change of energy levels induced by injected carriers occupying the molecular energy levels of pentacene [26]. As that, we may argue that the image of the relative change in the reflection intensity reflects the charge distribution along the FET channel. In experiment, CMR was measured at the gate voltage $V_{gs} = -40$ V (Fig. 3(a)) and $V_{gs} = +40$ V (Fig. 3(c)), with reference to the reflection image at $V_{ds} = V_{gs} = 0$ V. Figure 3(b) and (d) shows the signal modulation along the channel obtained by taking a line scan of the CMR image for $V_{gs} = -40$ V (Fig. 3(b)) and $V_{gs} = +40$ V (Fig. 3(d)). Since the light is completely reflected by Au, no modulation signal is detected at source and drain electrodes. Noteworthy, in the channel region the dark (black) region represents the increase of absorption ($-\Delta R/R > 0$) due to charge injection, whereas the bright (white) region represents the decrease of absorption due to charge depletion ($-\Delta R/R < 0$) [43]. As the I-V characteristics of Fig. 2 suggest that the polarization of P(VDF-TrFE) layer is pointing in the direction from pentacene to P(VDF-TrFE) at $V_{gs} = -40$ V, meanwhile from P(VDF-TrFE) to pentacene at $V_{gs} = +40$ V, we conclude that Figs. 3(a), (b) and (c), (d) display distributions of holes and electrons, respectively. That is, the results evidently show that holes and electrons are allowed to be injected into the channel, and that injected holes spread uniformly along the channel, while the spreading of electrons is confined in the region nearby source and drain electrodes. In other words, the electrostatic field caused from spontaneous polarization of P(VDF-TrFE) significantly contributes to hole and electron injection from electrodes into pentacene layer in the channel region. Noteworthy that many research groups have reported merely the possibility of electron injection into p-type pentacene FETs [52-54], but our CMR

imaging evidently supports their conclusions. It will be informative to discuss about CMR images we got in the region of gate voltage V_{gs} < coercive voltage V_c. At V_{gs} = -40 V shown in Fig. 3(a), CMR image of the channel region is bright ($\Delta R/R$ > 0), reflecting homogeneous hole distribution over the entire region of the channel. In the voltage region $V_{gs} < V_c$, CMR distribution is mostly the same but its intensity changes with increase of V_{gs}, indicating that holes spread over the channel on satisfying the relation $\Delta Q_s = C_g \Delta V_{gs}$ (C_g: gate insulator capacitance). On the other hand, at V_{gs} = +40 V shown in Fig. 3(c), CMR result showed that bright modulation signal is confined in the region nearby the source and drain electrode edge. In the voltage sweep from V_{gs} = +40 V until the voltage corresponding to the turn-over of spontaneous polarization $|V_{gs}| < |V_c|$, bright region of CMR image remains nearby source and drain electrode, and its intensity is getting weak as the gate voltage decreases. This means that electrons are distributed nearby source and drain electrode edge and the density of distributed electrons decreases in accordance with the gate voltage sweep from V_{gs} = +40 V to $|V_{gs}| = |V_c|$.

3-B-2 $V_{ds} = -15$ V

CMR image was captured to make clear the carrier distribution in the OFET channel under non-zero drain bias application ($V_{ds} = -15$ V). We here expected that the symmetric CMR image observed at $V_{ds} = 0$ V will be deformed, possibly due to asymmetric external electric field distribution and non-uniform turn-over of spontaneous polarization along the channel. The CMR imaging was carried out in the backward direction by applying gate bias from $V_{gs} = +40$ V to -40 V ($V_{ds} = -15$ V), where the reflection image at $V_{ds} = V_{gs} = 0$ V was the reference image. Figures 4(a)~(d) show the CMR images of the OFET channel at $V_{gs} = +40$ V (a), $V_{gs} = -15$ V (b), $V_{gs} = -23$ V (c), $V_{gs} = -40$ V (d), respectively. Note that these

images are changes of the image from the reference image. Figure 4(e) plots the signal modulation along the channel, which was obtained by a line scan of the CMR image. The dark region ($-\Delta R/R > 0$) represents charge injection into the energy states of pentacene, whereas the bright region ($-\Delta R/R < 0$) represents charge depletion from the energy states. Figure 4(a) is CMR image at $V_{gs} = +40$ V. Dark band region appears near the source and drain electrode edges, indicating the presence of injected electrons but it is limited to the channel region nearby source and drain electrodes. This situation is similar to the image of Fig. 3(c), which we got at V_{gs} = +40 V and V_{ds} = 0 V. With decreasing voltage V_{gs} from +40 V to -15 V, electrons in the channel near source and drain electrode edges are depleted. The electrostatic potential across the gate insulating layer is asymmetric at source and drain electrode due to nonzero drain-source voltage V_{ds} = -15 V. Consequently, electron density changes as $\Delta Q_s = C_g \Delta V_{gs}$ at source electrode, whereas $\Delta Q'_s = C_g(\Delta V_{gs} - V_{ds})$ at the drain electrode. As shown in Fig. 4(b), at V_{gs} = -15 V, electrons near source electrode is mostly depleted, resulting in a bright band of CMR image near source electrode. In the region nearby and under the source electrode, electric field is high and carrier injection is smooth. As the result, electrostatic potential across the ferroelectric layer is the same as the external applied voltage V_{gs}. Consequently, when the gate voltage exceeds coercive voltage V_c of the ferro-electric layer $V_{gs} > V_c$, polarization reversal occurs. On the other hand, in the central region of the FET channel, carriers are supplied from the source and drain edge region due to diffusion-drift motion of carriers. As the CMR image indicated, spontaneous polarization in this region is pointing from pentacene to P(VDF-TrFE) layer. In other words, negative polarization charge $-P_s$ is on the FET channel side of the ferroelectric layer while positive charge $+P_s$ is on the gate electrode side. The electrostatic field arising from the negative polarization charge in the channel region is repulsive for electrons migrating from the source electrode to the central region of the FET channel, and

pushing back electrons from the central region. This idea supports the observed CMR image indicating that injected electrons are confined near electrode region and not spreading into the central region of the channel. In further decreasing voltage to V_{gs} = -23 V (Fig. 4(c)), electrons are depleted on drain electrode side and holes are injected from source electrode, resulting bright band region near drain electrode edge in the CMR image. At V_{gs} = -40 V, holes spread over the FET channel region and give dark region in the CMR image, in a manner similar to Fig. 3(a). Noteworthy that the electron distribution at $V_{gs} = +40\ \mathrm{V}, V_{ds} = -15\ \mathrm{V}$ is very similar to that at $V_{gs} = +40\ \mathrm{V}, V_{ds} = 0\ \mathrm{V}$ (see Fig. 3(d)). Therefore, we may argue that the distribution of electrons around source electrode changes in the same way as that for $V_{ds} = 0\ \mathrm{V}$ with decrease in the applied gate voltage V_{gs}. That is, electrons at the source electrode will leave from the channel, on satisfying the relation $\Delta Q = C_g \Delta V$, where ΔV represents the change of voltage across the P(VDF-TrFE) layer under the source electrode. On the one hand, when the voltage across the P(VDF-TrFE) layer reaches the coercive voltage at $V_{gs} = V_A$, the polarization reversal occurs. In this situation, holes will be allowed to accumulate at the source electrode. It should be noted here that the turn-over of polarization still does not occur under the drain electrode owing to the applied potential difference of $V_{ds} = -15\ \mathrm{V}$ between source and drain electrodes. To induce turn-over of the polarization at the drain electrode, obviously we need to apply $V_{gs} = V_A - 15\ \mathrm{V}$. Actually in the I_{gs}-V_{gs} characteristics of Fig. 2(b), we can see two peaks at $V_{gs} = V_A$ and $V_{gs} = V_{A\prime}$, where the voltage difference between V_A and $V_{A\prime}$ is about 15 V ($= |V_{ds}|$). Noteworthy that we can discuss the two peak positions in the I_{gs}-V_{gs} characteristics for $V_{ds} = -5\ \mathrm{V}$ and $V_{ds} = -10\ \mathrm{V}$ in the same way. From the discussion above we may argue that decreasing V_{gs} leads to polarization reversal position shift toward the drain electrode, starting from the edge of the source electrode. Further we expect that when the turn-over occurs at the drain electrode, the OFET channel region will be filled with holes

gradually toward the drain electrode and the conductive carrier path is formed. Indeed, the drain current I_{ds} increases in two-step at the voltage corresponding to $V_{gs} = V_A$ and $V_{A'}$, respectively, and saturates as shown in Fig. 2(a). However, this is merely speculation. We can see the actual situation of this hole spreading process along the channel by using the CMR signal modulation plotted in Fig. 4(e). We found that holes spread gradually from the source electrode to the drain electrode along the channel.

To further clarify the details of above discussion on carrier spreading in terms of polarization reversal process, we analyzed the results on the basis of transmission line model, basically an extension of the Maxwell-Wagner effect element analysis [55]. According to this model, when charge carriers are injected into the OFET channel and channels are filled with carriers, potential $V(x)$ in steady state is described as

$$V(x) = \left(V_{gs} - V_{ds}\right) + V_{ds}\sqrt{\frac{x}{L}} \qquad \cdots(1)$$

Here, $x = 0$ and $x = L$ correspond to the edges of the drain and source electrodes, respectively. V_{ds} is the potential difference between the source and drain electrodes. Therefore, the carrier accumulates along the channel on satisfying the square root dependence on x due to the potential difference. This situation appears for $V_{ds} = -15\,\mathrm{V}$ as plotted in Fig. 4(e) by a dashed curve, and experimental result of CMR well accounts for this relation. By the way, carriers accumulated at the pentacene/P(VDF-TrFE) interface should be given by the sum of the charge accumulated due to the spontaneous polarization P_0 of P(VDF-TrFE) and the charge $C_g V(x)$ due to the potential built along the channel between source and drain. For our samples, spontaneous polarization was $10\,\mu\mathrm{C/cm^2}$, while the capacitance C_g of P(VDF-TrFE) layer

was 3.3×10^{-8} F/cm^2 and the $C_g V_{gs}$ was around 0.50 μC/cm^2 for $V_{gs} = -15$ V. In other words, the accumulated charge density is mainly dependent on the turn-over of the spontaneous polarization. It is interesting here to discuss the position of polarization reversal in terms of the potential distribution $V(x)$. As $V(x)$ represents the voltage across the P(VDF-TrFE) layer, it is reasonable to consider that polarization reversal occurs at the point where $V(x)$ is reaching the coercive voltage of P(VDF-TrFE) layer.

Figure 5 shows calculation (solid line) and CMR results (symbols) of the position of polarization reversal in the channel. As shown by CMR imaging in Fig. 4, in decreasing V_{gs} from V_A, holes spread to the center region of the FET channel and its frontier reached at $x = 11$ μm. Consequently, in the voltage region $V_{A'} < V_{gs} < V_A$, polarization reversal position x shifts from the center region ($x = 11$ μm) toward the drain electrode edge ($x = 0$) with satisfying the relationship of Eq. (1). This calculation coincides well with the results, indicating that polarization reversal position shifts due to the change of potential distribution along the channel.

4. Conclusion

By using charge modulated reflectance imaging technique, we studied charge distribution and polarization reversal process in the pentacene OFET with a P(VDF-TrFE) ferroelectric gate insulator. The modulated signal represents the charge injection into pentacene layer, and the signal from the channel well traces the carrier distribution. Results showed that both holes and electrons can enter into pentacene layer. Injected holes distribute over the entire channel region, on the other hand, electrons are confined in the region nearby source and drain electrodes. This is caused by the difference of electrostatic field induced from the spontaneous polarization of P(VDF-TrFE). In the OFET structure, polarization reversal of P(VDF-TrFE) layer occurs in the

OFET channel, but the reversal position shifts along the channel from the source to the drain, followed by the accumulation of holes that are injected from the source electrode. CMR imaging results clarified that carrier spreading and polarization reversal process in OFET with ferroelectric gate insulator can be explained based on the MW effect.

References

[1] T. Sekitani and T. Someya, ***Jpn. J. Appl. Phys.***, 51, 100001/1-13 (2012).

[2] T. Tsujimura, *OLED displays: fundamentals and applications* (Wiley, New Jersey, 2012).

[3] M. Pagliaro, G. Palmisano, and R. Ciriminna, *Flexible solar cells* (Wiley, Weinheim, 2008).

[4] Y. J. Park, I.-S. Bae, S. J. Kang, J. Chang, and C. Park, ***IEEE Trans. Dielectr. Electr. Insul.***, 17, 1135-1163 (2010).

[5] G. Meller, T. Grasser, *Organic electronics* (Springer, Berlin, 2010).

[6] A. Köhler, H. Bässler, *Electronic processes in organic semiconductors: An introduction* (Wiley, Weinheim, 2015).

[7] K. Kudo, M. Yamashina, and T. Moriizumi, ***Jpn. J. Appl. Phys.***, 23, 130 (1984); H. Koezuka, A. Tsumura, and T. Ando, ***Synth. Met.***, 18, 699–704 (1987); M. L. Petrova L. D. Rozenshtein, ***Sov. Phys.,*** 12, 961-962, translated from F*izika Tverdogo Tela.* (1969).

[8] H. Sirringhaus, ***Adv. Mater.,*** 26, 1319-1335 (2014); Q.-F. Li, S. Liu, H. -Z. Chen, H. –Y. Li, ***Chin. Chem. Lett.***, 27, 1421-1428 (2016).

[9] H. Iino, T. Usui, and J. Hanna, ***Nat. Commun.***, 6, 6828 (2015).

[10] S. Ogawa Ed, *Organic electronics materials and devices* (Springer, Tokyo, 2015).

[11] M. Iwamoto, T. Manaka, and D. Taguchi, ***J. Phys. D: Appl. Phys.***, 48, 373001/1-20 (2015).

[12] M. Weis, D. Taguchi, T. Manaka and M. Iwamoto, , ***Jpn. J. Appl. Phys.***, 49, 04DK15/1-5 (2010).

[13] E. Lim, T. Manaka, R. Tamura, M. Iwamoto, ***Curr. Appl. Phys.***, 7, 356-359 (2007).

[14] For example, S. M. Sze, *Physics of Semiconductor Devices, 2nd ed.* (Wiley-Interscience, New York, 1981).

[15] E. Lim, T. Manaka, and M. Iwamoto, ***J. Appl. Phys.***, 104, 5, 54511 (2008).

[16] D. Taguchi, L. Zhang, L. Jun, W. Martin, T. Manaka, and M. Iwamoto, ***J. Phys. Chem. C***, 114, 35, 15136–15140 (2010).

[17] R. Tamura, E. Lim, T. Manaka, and M. Iwamoto, ***J. Appl. Phys.***, 100, 11, 114515(2006).

[18] Y. Mashiko, D. Taguchi, M. Weis, T. Manaka, and M. Iwamoto, ***Appl. Phys. Lett.***, 101, 24, 243302 (2012).

[19] M. Weis, J. Lin, D. Taguchi, T. Manaka, and M. Iwamoto, ***Jpn. J. Appl. Phys.***, 49, 7, 71603 (2010).

[20] T. Manaka, E. Lim, R. Tamura, M. Iwamoto, ***Nat. Photonics***, 1, 581-584 (2007).

[21] E. Lim, T. Manaka, M. Iwamoto, ***J. Appl. Phys.***, 101, 024515/1-6 (2007).

[22] M. Iwamoto, T. Manaka, D. Taguchi, ***IEEJ Trans. on Fundamentals and Materials***, 136, 678-684 (2016). [in Japanese]

[23] D. Taguchi, M. Weis, T. Manaka, M. Iwamoto, ***Appl. Phys. Lett.,*** 95, 263310/1-3 (2010).

[24] D. Taguchi, L. Zhang, J. Li, M. Weis, T. Manaka, M. Iwamoto, ***J. Phys. Chem. C***, 114, 15136-15140 (2010).

[25] A. Sadakata, K. Osada, D. Taguchi, T. Yamamoto, M. Fukuzawa, T. Manaka, and M. Iwamoto, ***J. Appl. Phys.***, 112, 083723/1-8 (2012).

[26] T. Otsuka, D. Taguchi, T. Manaka, and M. Iwamoto, ***J. Appl. Phys.***, 121, 6, 65501 (2017).

[27] J. Li, M. Weis, D. Taguchi, T. Manaka, and M. Iwamoto, ***J. Appl. Phys.***, 111, 2, 23706 (2012).

[28] Z. Shi, D. Taguchi, T. Manaka, and M. Iwamoto, ***J. Appl. Phys.***, 119, 165502/1-7 (2016).

[29] X. Cui, D. Taguchi, T. Manaka, and M. Iwamoto, ***J. Appl. Phys.***, 114, 23, 234504 (2013).

[30] R. Tamura, S. Yoshita, E. Lim, T. Manaka, M. Iwamoto, ***Jpn. J. Appl. Phys.***, 47, 3170–3173 (2008).

[31] R. Tamura, S. Yoshita, E. Lim, T. Manaka, M. Iwamoto, ***Jpn. J. Appl. Phys.***, 47, 476-479

(2008).

[32] R. Tamura, S. Yoshita, E. Lim, T. Manaka, M. Iwamoto, ***Jpn. J. Appl. Phys.***, 47, 3170-3173 (2008).

[33] S. Yoshita, R. Tamura, D. Taguchi, M. Weis, E. Lim, T. Manaka, and M. Iwamoto, ***J. Appl. Phys.***, 106, 024505/1-4 (2009).

[34] T. Cramer, L. Travaglini, S. Lai, L. Patruno, S. de Miranda, A. Bonfiglio, P. Cosseddu, and B. Fraboni, ***Scientific Reports***, 6, 38203/1-9 (2016).

[35] L. Bürge, H. Sirringhaus, R. H. Friend, ***Appl. Phys. Lett.***, 80, 2913-2915 (2002).

[36] S. Ikeda, T. Shimada, M. Kiguchi, K. Saiki, ***J. Appl. Phys.***, 101, 094509/1-8 (2007).

[37] W. W. A. Koopman, S. Toffanin, M. Natali, S. Troisi, R. Capelli, V. Biondo, A. Stefani, and M. Muccini, ***Nano Lett.***, 14, 1695-1700 (2014).

[38] H. Matsui, T. Hasegawa, ***Appl. Phys. Lett.***, 95, 223301/1-3 (2009).

[39] K. Lee, H. Melikyan, A. Babajanyan, B. Friedman, *Near-field microwave microscopy for nanoscience in B. Bhushan ed, Scanning probe microscopy in nanoscience and nanotechnology, vol.2*, (Springer, Berlin, 2011) Chap 5.

[40] T. Verbiest, K. Clays, V. Rodriguez, *Second-order Nonlinear Optical Characterization Techniques: An Introduction* (CRC, New York, 2009). Chap 5 and 6.

[41] G. Horowitz, Interfaces in *Organic field-effect transistors*, in G. Meller, T. Grasser Eds, *Organic electronics* (Springer, Berlin, 2010).

[42] M. Weis, T. Manaka, M. Iwamoto, *Analysis of contact resistance and space-charge effects in organic field-effect transistors*, in M. Iwamoto, Y. -S. Kwon, T. Lee Eds, *Nanoscale interface for organic electronics* (World Scientific, Singapore, 2011). Chap. 2.

[43] T. Manaka, S. Kawashima, M. Iwamoto, ***Appl. Phys. Lett.***, 97, 113302/1-3 (2010).

[44] A. R. Davis, L. N. Pye, N. Katz, J. A. Hudgings, K. R. Carter, ***Adv. Mater.***, 26, 4539-4545

(2014).

[45] Z. Q. Li, G. M. Wang, N. Sai, D. Moses, M. C. Martin, M. Di Ventra, A. J. Heeger, and D. N. Basov, ***Nano. Lett.,*** 6, 224-228 (2006).

[46] T. Yagi, M. Tatemoto, and J. Sako, ***Polymer Journal***, 12, 4. 209–223 (1980).

[47] N. Yamauchi, ***Jpn. J. Appl. Phys.***, 25, 4, 590–594 (1986).

[48] J. H. Burroughes, C. A. Jones, and R. H. Friend, ***Nature***, 335, 137–141 (1988).

[49] P. J. Brown, H. Sirringhaus, M. Harrison, M. Shkunov, and R. H. Friend, ***Phys. Rev. B***, 63, 12, 125204 (2001).

[50] M. Cardona, *Modulations Spectroscopy* (Academic, New York, 1969).

[51] J. Li, D. Taguchi, W. OuYang, T. Manaka, and M. Iwamoto, **Appl. Phys. Lett.**, 99, 6, 063302 (2011).

[52] M. Ahles, R. Schmechel, and H. Von Seggern, ***Appl. Phys. Lett.***, 85, 19, 4499–4501 (2004).

[53] T. Yasuda, T. Goto, K. Fujita, and T. Tsutsui, ***Appl. Phys. Lett.***, 85, 11, 2098–2100 (2004).

[54] S. Takebayashi, S. Abe, K. Saiki, and K. Ueno, ***Appl. Phys. Lett.***, 94, 8, 8–10 (2009).

[55] M. Weis, T. Manaka, and M. Iwamoto, ***J. Appl. Phys.***, 105, 2, 24505 (2009).

Figure captions

Figure 1: (a) Device structure of pentacene FET with a ferroelectric gate insulator (P(VDF-TrFE)) and experimental setup for CMR imaging measurement. (b) Absorption spectrum of a pentacene film (200 nm) and a P(VDF-TrFE) film (200 nm).

Figure 2: (a) The drain current-gate voltage (I_{ds}-V_{gs}) characteristics and (b) gate current-gate voltage (I_{gs}-V_{gs}) characteristics of FET with varied V_{ds} as a parameter. The channel length L and width W of FET is $50\ \mu m$ and $2\ mm$, respectively. (c) Electron and hole distribution and polarization distribution in the I-V measurement at V_{ds} = -15 V.

Figure 3: (a) Modulated reflectance ($\Delta R/R$) image from the FET channel and (b) reflectance change along the channel length direction at $V_{gs} = -40\ V$ ($V_{ds} = 0\ V$). (c) Modulated reflectance ($\Delta R/R$) image from the FET channel and (d) reflectance change along the channel length direction at $V_{gs} = +40\ V$ ($V_{ds} = 0\ V$).

Figure 4: Modulated reflectance ($\Delta R/R$) image from the FET channel at $V_{gs} = +40\ V$(a), $V_{gs} = -15\ V$ (b), $V_{gs} = -23\ V$ (c), $V_{gs} = -40\ V$ (d) ($V_{ds} = -15\ V$) and signal modulation along the channel obtained by taking a line scan of the CMR image (e). Dashed curve represents the potential distribution for $V_{gs} = -40\ V$ obtained from Eq. (1).

Figure 5: The position of polarization reversal in the channel. The solid line depicts the calculation based on Eq. (1) and the symbols represent experimental results from CMR imaging.

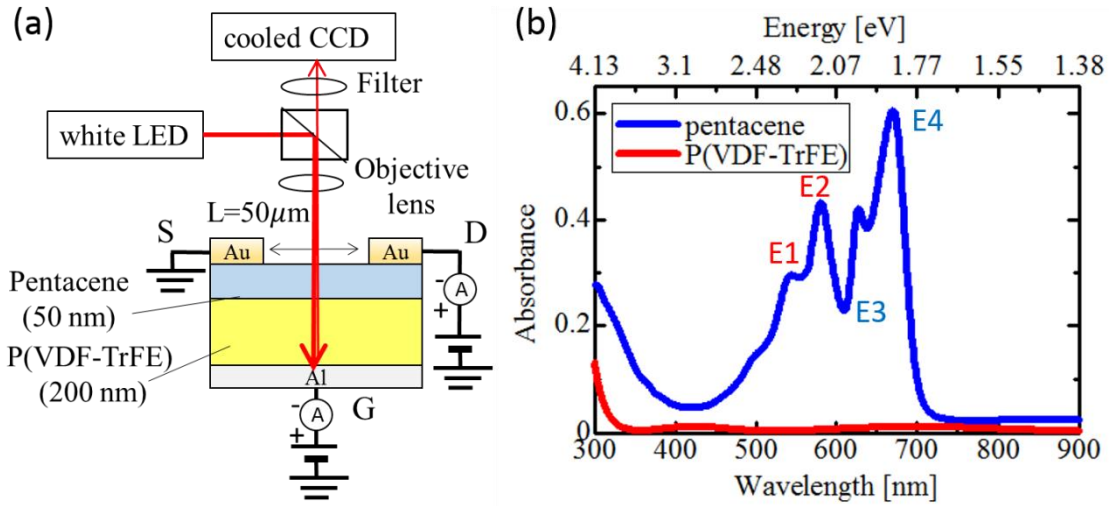

Fig. 1: T. Otsuka et al.

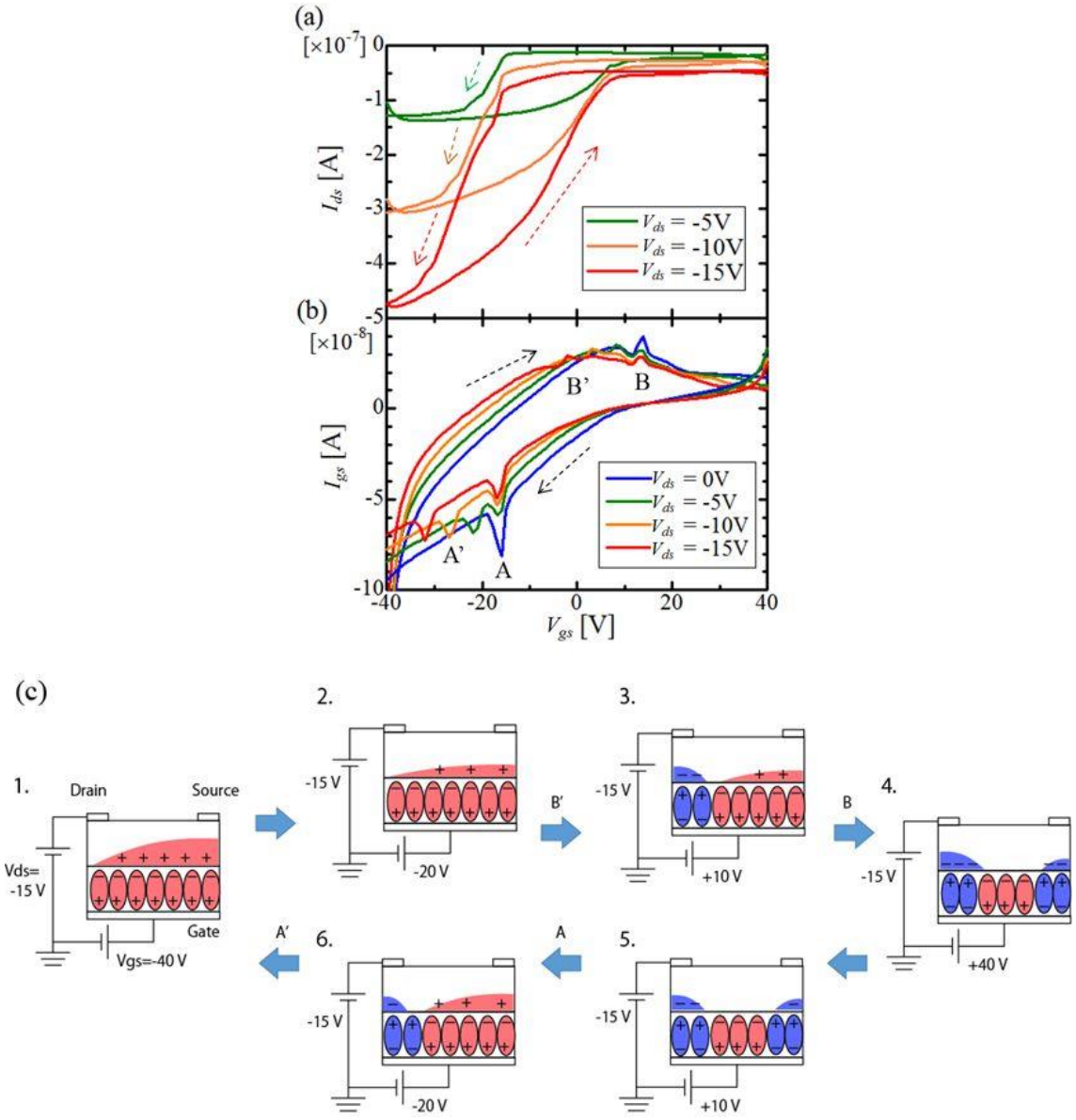

Fig. 2: T. Otsuka et al.

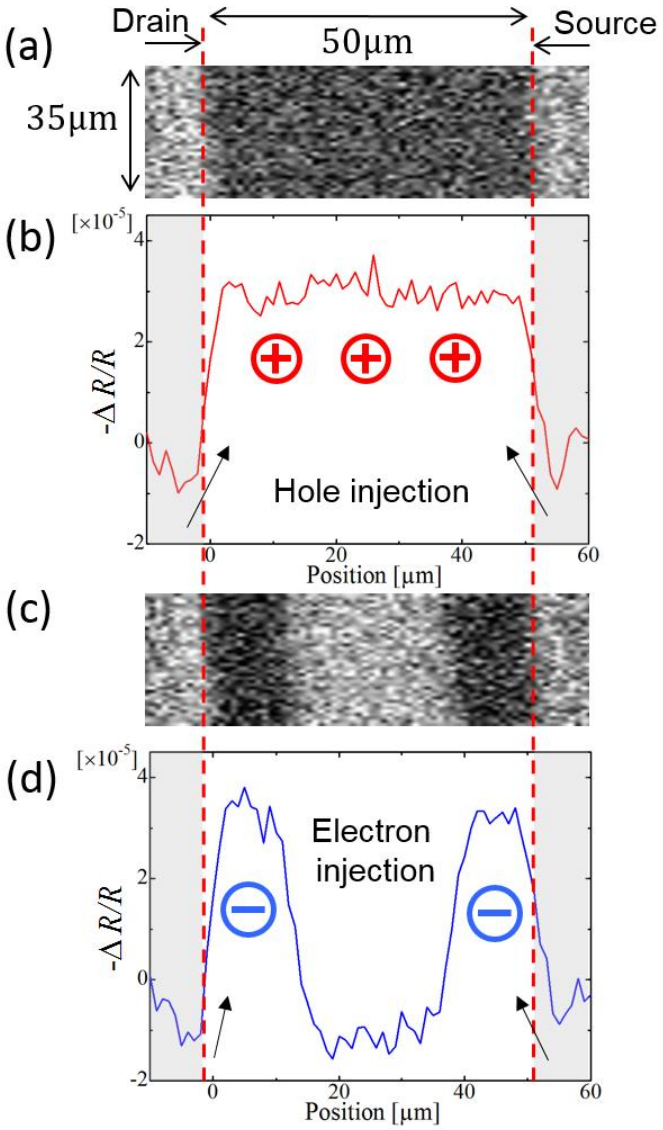

Fig. 3: T. Otsuka et al.

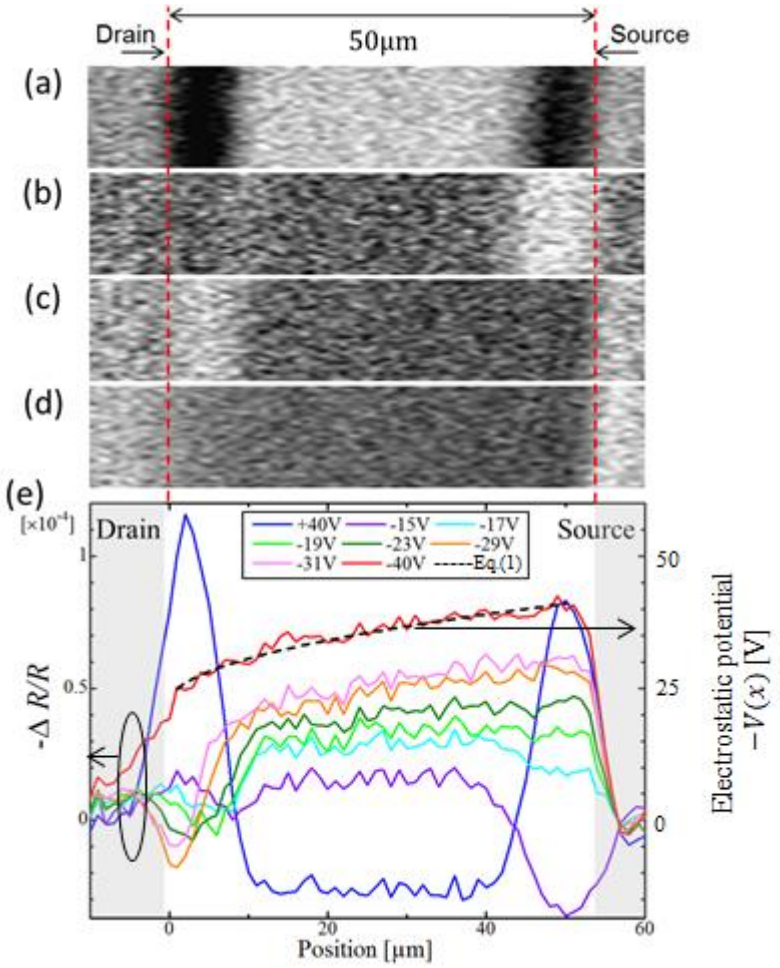

Fig. 4: T. Otsuka et al.

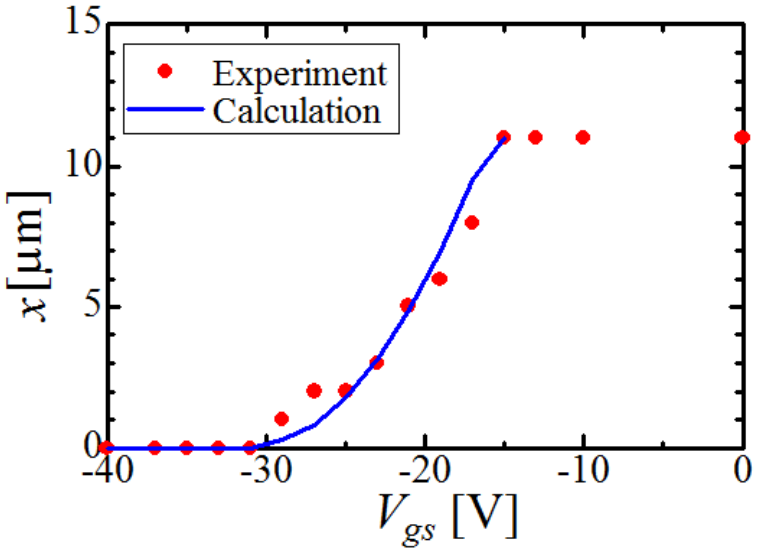

Fig. 5: T. Otsuka et al.